Journal of Materials Science: Materials in Electronics (2018) 29:18978–18988
https://doi.org/10.1007/s10854-018-0022-0

Dielectric loss models, relaxor behavior and high ferroelectric properties of BCZTS-*x*ST ceramics

Fangfang Zeng[1] · Qibin Liu[1,2] · Yuanyu Wang[1] · Shiqiang Peng[1] · An Xue[1] · Enpei Cai[1]

Received: 29 July 2018 / Accepted: 6 September 2018 / Published online: 18 September 2018

Abstract
In the work, the preparation technology of $SrTiO_3$ is carefully investigated. The $(Ba_{0.85}Ca_{0.15})(Zr_{0.08}Ti_{0.9}Sn_{0.02})O_3$-$SrTiO_3$ piezoelectric ceramics are successfully synthesized by conventional solid-state reaction method, and the microstructure, ferroelectric and dielectric properties are studied in detail. The excellent ferroelectric properties are obtained when $x = 20$ wt.% (P_r and E_c are 11.67 μC/cm^2 and 2.06 kV/mm, respectively). In addition, the Curie temperature is 114 °C at $x = 5$ wt.%. The dielectric permittivity ε_r, dielectric loss $tan\delta$ and relaxor behavior are investigated in the work. In particular, two dielectric loss peaks, Model A and Model B, are systematically discussed.

1 Introduction

Recently, piezoelectric ceramics which are widely used in variety of fields, such as super-conducting, power engineering, consumer electronics and actuators, have attracted extensive attention [1–5]. Lead-based piezoelectric ceramics are very important piezoceramics, while lead (Pb) is toxic and harmful to environment. With increasing worldwide concern for the safety issues, some researchers are exploring a series of Pb-free piezoelectric ceramics to displace lead-based piezoelectric ceramics, such as $BaTiO_3$ (BT) [6, 7], $BiFeO_3$ (BFO) [8] $K_{0.5}Na_{0.5}NbO_3$ (KNN) [9] and $Bi_{0.5}Na_{0.5}TiO_3$ (BNT) [10]. Recently, some progresses have been made by Wu et al. to improve lead-free piezoelectric properties [11, 12]. Unfortunately, parts of their properties are not very ideal for application. Therefore, many efforts have been made to enhance the properties of lead-free piezoceramics through dopants [13–22], advancing sintering technology [23–25] and fabrication textured ceramics [23–25].

Recently, relaxor ferroelectrics are extensively used in high performance sensors, hysteresis-free actuators and multilayer ceramics capacitors due to their excellent dielectric and piezoelectric performance [1–3]. Meanwhile, increasing attention has been paid to BCZT-based ceramics because of their relatively high piezoelectric performance (d_{33} ~ 620 pC/N) [22]. However, the Curie temperature of $BaTiO_3$-based (< 93 °C) is not high enough to be used at high temperature [22]. Therefore, a great number of efforts have been made to develop the relaxor ferroelectrics for high temperature application. Due to $SrTiO_3$ widely used to prepare relaxor ferroelectrics [26–28]. Hence, $SrTiO_3$ is introduced into BCZT-based ceramics in the work in order to improve the relaxor ferroelectrics performances of the ceramics. Furthermore, the dielectric loss model of $(Ba_{0.85}Ca_{0.15})(Zr_{0.08}Ti_{0.9}Sn_{0.02})O_3$-$xSrTiO_3$ ceramics is rarely mentioned in recent years. Therefore, the dielectric loss model is studied in depth. In addition, the relaxor behavior and ferroelectric properties are also discussed in this work.

2 Experiment

It is difficult to directly synthesize the $SrTiO_3$ (ST), so the two-step molten-salt method was used in the work [27, 30].

Figure 1 is schematic diagram of preparation process of the ST. In the first step, $SrCO_3$ and TiO_2 (3.2:2) were mixed firstly, and the powders were ball-milled for 3 h. Afterwards, NaCl and KCl were added to the powders and ball-milled for 1 h again. The suspension was filtered by the sieve of 80 meshes after dried, and sintered for 3 h at 1000 °C. The calcined powder was rinsed by deionized water of 80 °C until the white

✉ Qibin Liu
qbliugzu@163.com

[1] College of Material and Metallurgy, Guizhou University, Guiyang 550025, Guizhou, People's Republic of China

[2] Key Laboratory for Material Structure and Strength of Guizhou Province, Guiyang 550025, Guizhou, People's Republic of China

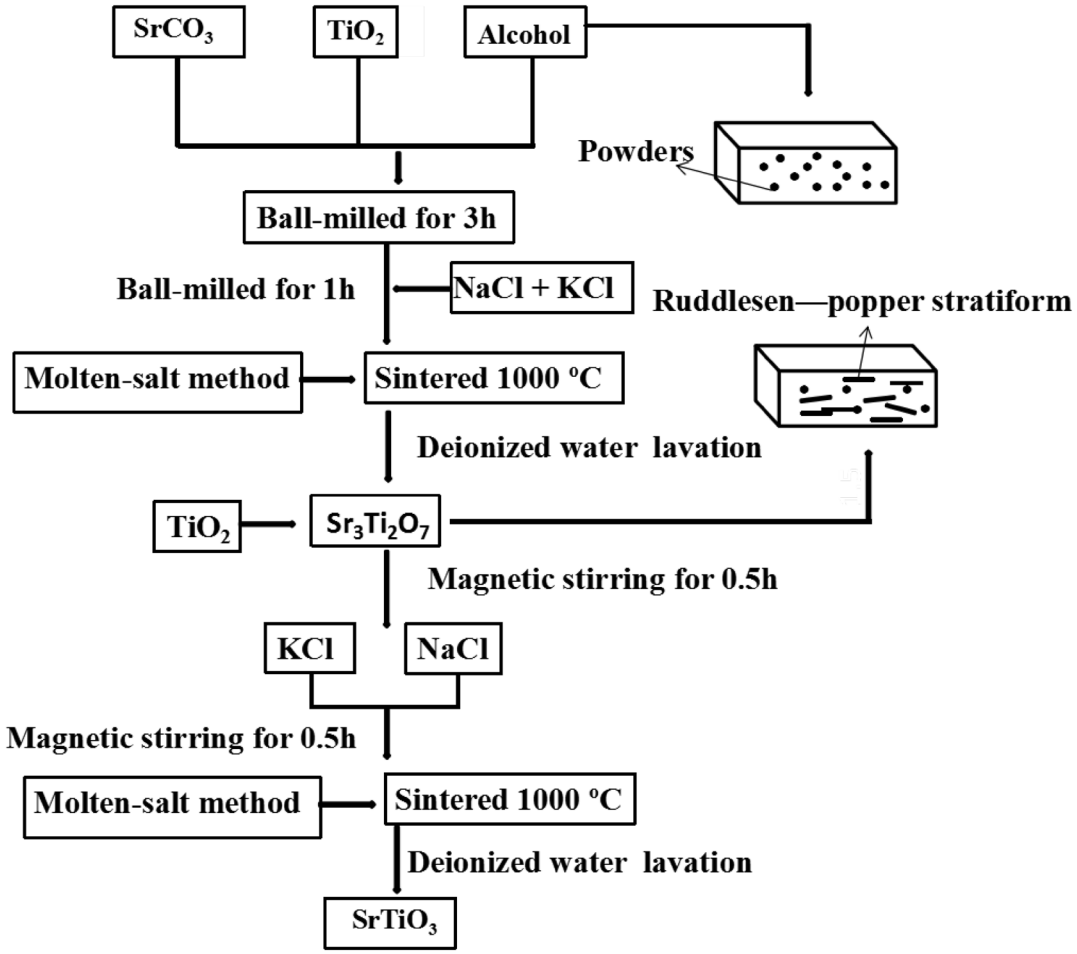

Fig. 1 The schematic is the preparation technique of $SrTiO_3$

precipitate AgCl was not observed ($AgNO_3$ was detection reagent). The obtained powders were intermediate product $Sr_3Ti_2O_7$, and the synthesis formula of $Sr_3Ti_2O_7$ is presented:

$$3SrCO_3 + TiO_2 \xrightarrow{NaCl+KCl} Sr_3Ti_2O_7 \quad (1)$$

In the second step, the intermediate product $Sr_3Ti_2O_7$ was mixed with TiO_2 by the mole ratio of 1.0:1.1, using magnetic stirring apparatus to stir in alcohol medium for 0.5 h. Thereafter, NaCl and KCl were added to the mixture by a half of total mass of $Sr_3Ti_2O_7$ and TiO_2, and the suspension was stirred by magnetic stirring apparatus for 0.5 h again. After sintered for 3 h at 1000 °C. The powder was rinsed by deionized water of 80 °C until the white sediment (AgCl) was not observed. Finally, the obtained powders were $SrTiO_3$, and the synthesis formula of $SrTiO_3$ as follows:

$$Sr_3Ti_2O_7 + TiO_2 \xrightarrow{NaCl+KCl} 3SrTiO_3 \quad (2)$$

The raw materials of $(Ba_{0.85}Ca_{0.15})(Zr_{0.08}Ti_{0.9}Sn_{0.02})O_3$ (abbreviated as BCZTS) were composed of carbonates and oxides. $BaCO_3$, $CaCO_3$, ZrO_2, TiO_2, SnO_2, $SrCO_3$, were mixed according to appropriate stoichiometric ratio and ball-milled for 12 h, then calcined for 3 h by conventional solid-state reaction method. The $SrTiO_3$ and the prepared matrix were mixed and ball-milled for 12 h. These dried powders were mixed with 6 wt.% paraffin and pressed into pellets of 12 mm in diameter and 1 mm in thickness, and the green pellets were heated for 1 h at 600 °C for binder removal and sintered for 3 h at 1310 °C.

Phase composition of sintered samples was detected by X-ray diffraction (XRD) with a Cu K_α radiation (X'pert-PRO X-ray diffraction, PANAlytical Company, The Netherlands). The microstructure of sintered bulks was observed by scanning electron microscope (SEM) (JSM-5900, Japan Electronics Corporation), and dielectric properties were measured by a LCR meter (TH2618B, Guangzhou Zhuo Yue electronic instrument and Equipment Co., Ltd.) at various frequencies in the temperature range 0–300 °C. The ferroelectric properties were measured by hysteresis loop measuring instrument (RT66A; Radiant Technologies Inc., Albuquerque, NM) at room temperature.

3 Results and discussions

3.1 Phase composition and microstructure

Figure 2 is the surface morphologies of BCZTS-*x*ST ceramics. It was observed that the grain size firstly decreased, then increased. When 0 wt.% ≤ x ≤ 20 wt.%, the grain became small gradually with the increase of x, and gradually increased again when x > 20 wt%. The reason that the grain becomes much small with the increase of x is probable the ST stockpiling in the grain boundary and suppressing the grain growth [18, 31]. However, excess doping resulted in grain growth again when 20 wt.% ≤ x ≤ 50 wt.%, and resulting in the coarse grain. It might be the successive shrinkage of pore in the grain boundary, and leading to the decreasing of binding energy of interface and pore. The pore and interface separate and move ahead when the binding energy reached a limit value, which resulted in the grain abnormal growth [32].

Figure 3 shows the X-ray diffraction spectrum of the BCZTS-*x*ST samples in the 2θ range of 5°–85° and enlarged XRD patterns of 44°–47° and 30.5°–32.5°, respectively. It is observed from Fig. 3 that all samples exhibit a pure perovskite without secondary phase except the x = 40 wt.% and 50 wt.%. The perovskite structure can be verified by the formula (3). And it is also seen that second phase appeared at x = 5 wt.% and 20 wt.% in Fig. 3b. Through the PANalytical HighScore analysis, the second phase is mid-body $Sr_3Ti_2O_7$.

$$R_A + R_O = t\sqrt{2}(R_B + R_O) \tag{3}$$

Where the R_A and R_B are cation radius of A site and B site, respectively. R_O and t refer to oxygen-ion radius and the Goldschmidt tolerance factor [4], respectively. It is perovskite structure when tolerance factor t in the range of 0.9 to 1.1. According to the formula (3), t is equal to 1.03, indicating that the samples are perovskite structure. It can be observed from Fig. 3c that the peaks (002) shifted to a low angle with increasing ST, and then gradually shifted to a higher angle at x ≥ 20 wt.%. It can be explained by Bragg's law. The radius of Sr^{2+} and Sn^{4+} are 1.12 Å and 0.69 Å, respectively. It is observed from Fig. 3c that the diffraction peak shifted slightly towards low angles with the increase of ST (x ≤ 10 wt.%). It's probably due to the fact that Sn^{4+} and Sr^{2+} ions entered into B and A site and dominatingly substituted Ti^{4+}(0.60 Å) and Ca^{2+}(1.06 Å), resulting in the expansion of crystal lattice and consequently shifts of (002) peak to a lower angle. The peak obviously shifts to higher angle at x ≥ 20 wt.%, and the reason is that the substitution of Sn^{4+}(0.69 Å) and Sr^{2+}(1.12 Å) for Ti^{4+}(0.60 Å) and Ca^{2+}(1.06 Å) have reached saturated state. Therefore, the Sn^{4+}(0.69 Å) and Sr^{2+}(1.12 Å) substituting Zr^{4+}(0.72 Å) and Ba^{2+}(1.38 Å) is dominated, respectively, when x ≥ 20 wt.%.

3.2 The ferroelectric properties and dielectric loss models

It is observed from Fig. 4 that the maximum remnant polarization (P_r) and the coercive field (E_c) were 11.67 μC/cm^2 and 2.06 kV/mm when x = 20 wt.%. With increasing of $SrTiO_3$ content, it can be observed from the inset that the change of P_r and E_c were wave-like. The hysteresis loops are not saturated for all samples because of low density and porosity in the ceramics [33, 34]. The reason that the remnant polarization is the maximum at x = 20 wt.% is mainly because of efficient 180° domain wall [32], and the enhanced P_r should be due to the lossy properties, such as space charge and dipole rotation.

The temperature dependence of dielectric constant and loss for the $(Ba_{0.85}Ca_{0.15})(Zr_{0.08}Ti_{0.9}Sn_{0.02})O_3$-$x$SrTiO$_3$

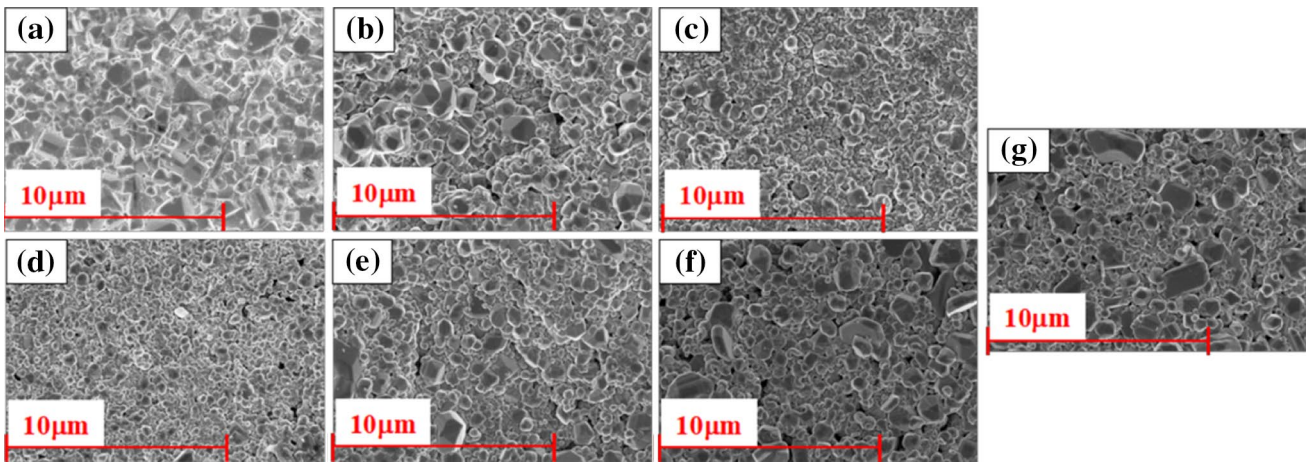

Fig. 2 The SEM images of $(Ba_{0.85}Ca_{0.15})(Zr_{0.08}Ti_{0.9}Sn_{0.02})O_3$-$x$SrTiO$_3$ ceramic. **a** x = 0, **b** x = 5 wt.%, **c** x = 10 wt.%, **d** x = 20 wt.%, **e** x = 30 wt.%, **f** x = 40 wt.%, **g** x = 50 wt.%

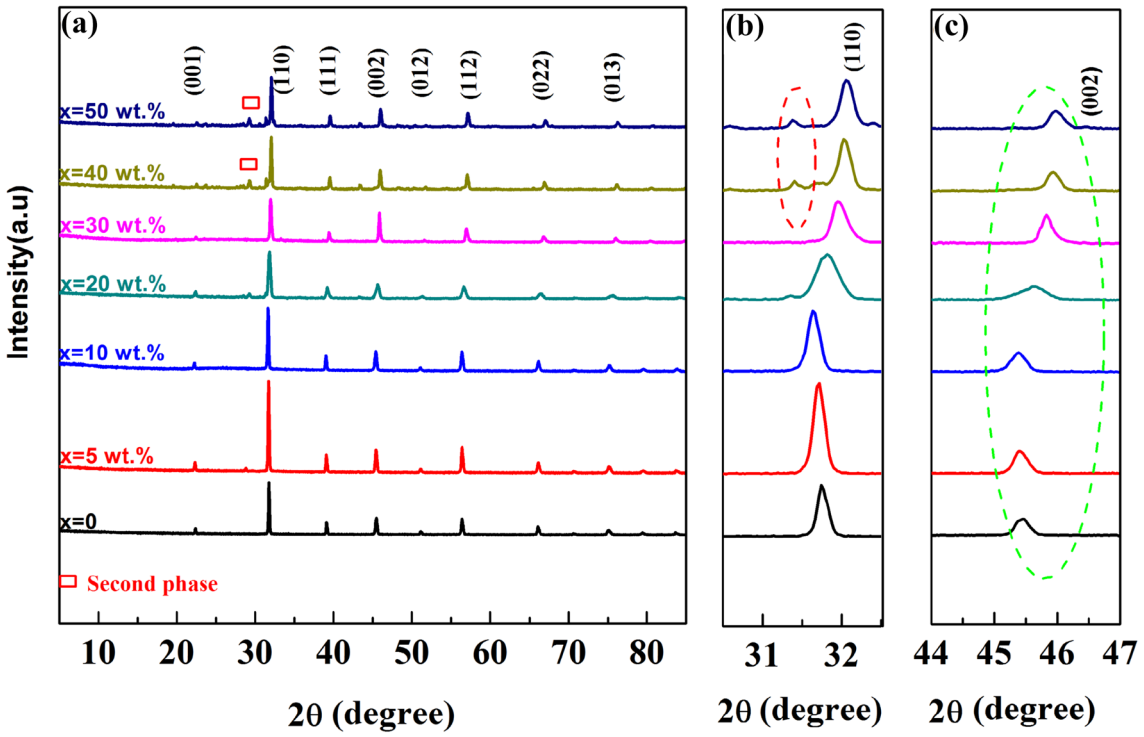

Fig. 3 **a** XRD patterns and expanded XRD patterns with 2θ ranging from **b** 30.5°–32.5° and **c** 44°–47° of $(Ba_{0.85}Ca_{0.15})(Zr_{0.08}Ti_{0.9}Sn_{0.02})O_3$-$x$Sr-$TiO_3$ samples as a function of x

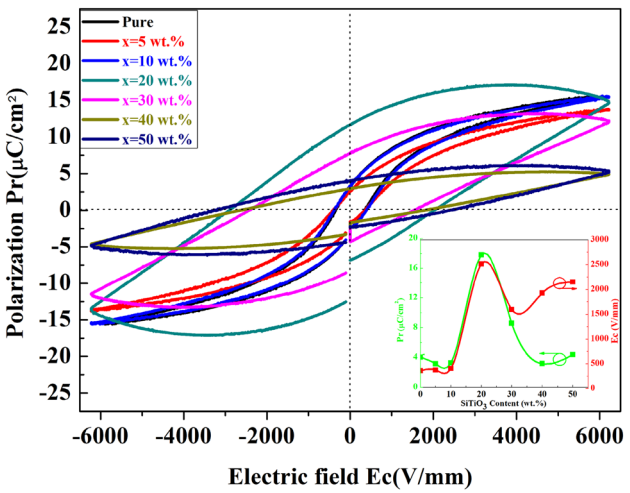

Fig. 4 Exhibition the polarization hysteresis hoops of the $Ba_{0.85}Ca_{0.15}Zr_{0.08}Ti_{0.9}S_{0.02}$-$x$ST specimens as a function of electric field, and the inset photo is the remnant polarization and coercive field as a function of x content

ceramics at a frequency of 100 Hz is shown in Fig. 5a, and the dielectric loss peaks of Model A and Model B with various $SrTiO_3$ contents are exhibited in Fig. 5b. Figure 5c shows the enlarged curves of Model A and Model B. The inset shows temperature dependence of dielectric loss with various frequencies, and Model A and Model B are observed at $x \geq 20$ wt.% in Fig. 5c. Model A and Model B appeared around 25 °C and 250 °C, respectively. These models are called relaxation model. The relaxation models A (70 K) and B (150 K) had been also observed in $SrTiO_3$ thin films [35], $(1-x)$BNKLLT-xBCZT ceramics [36], polycrystalline samples [37], and single crystals [38].

Some researchers thought that the relaxation model was a static response rather than dynamic response. However, it is obviously observed from Fig. 5c that Model A has shown a dynamic response. Someone thought the anomalies of dielectric curve was related to the thermal evolution of relaxation time distribution or correlation length distribution of the polar nanoregions (PNRs), which had nothing to do with the measurable phase transition [36, 39, 40]. The excessive ions have segregated at the grain boundary, which resulted in the formation of dielectric loss peaks [15]. Furthermore, the point defects of cation (interstitials, vacancies and impurities) were responsible for the dielectric loss peaks. At low temperature, the dielectric loss peak was similar with the results in single crystal. Moreover, it was also related to the defect model and the soft model [31, 35, 37, 41].

Besides, an intrinsic mechanism should be involved. As is well-known, $SrTiO_3$ is a typical soft model quantum paraelectrics, which interacts with point defects of cation at low temperature. The similar phenomenon was investigated

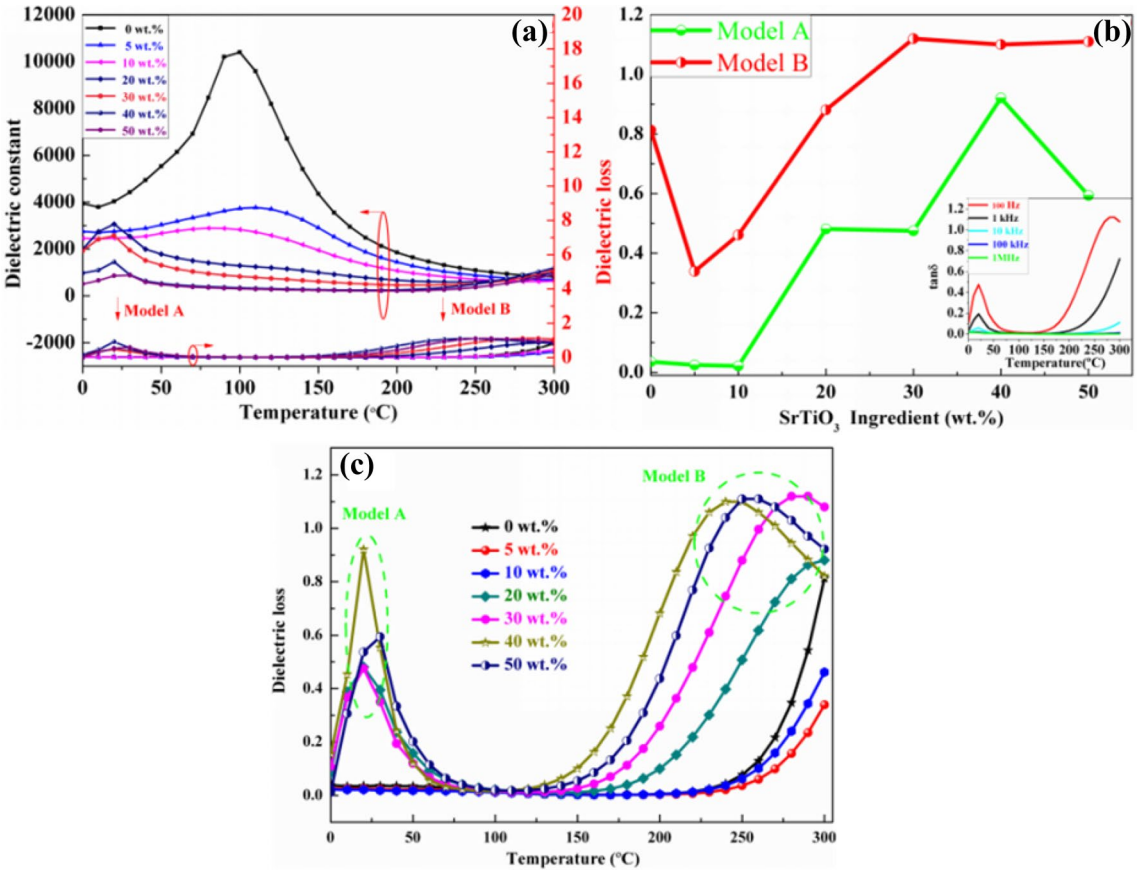

Fig. 5 **a** Shows the temperature dependence of dielectric constant and loss of $(Ba_{0.85}Ca_{0.15})(Zr_{0.08}Ti_{0.9}Sn_{0.02})O_3$-$x$$SrTiO_3$ ceramics at a frequency of 100 Hz, **b** exhibits $SrTiO_3$ content dependence of dielectric loss for $Ba_{0.85}Ca_{0.15}Zr_{0.08}Ti_{0.9}Sn_{0.02}$-$x$$SrTiO_3$ ceramics, and **c** shows the enlarged figure of Model A and Model B. The inset of b shows temperature-dependent dielectric loss with various frequencies

in many literatures [37]. The maximum value of Model A is observed at $x = 40$ wt.% in Fig. 5b, suggesting that the defects and vacancies were the maximum at $x = 40$ wt.%. For Model B, it was considered that the dielectric loss peak was related to oxygen vacancies and the rerotation of Ti^{4+} at high temperature. The formation of oxygen vacancies may be due to variety of reasons such as pressure deviations or annealing ratio etc., and long-playing annealing was the most important one among these reasons. The different degree of congregation of oxygen vacancies and the rerotation of Ti^{4+} at high temperature resulted in the dielectric loss peak [35, 37, 41]. In addition, it was related to defects and soft model [31].

It is observed from the inset of Fig. 5b that the dielectric loss disappeared gradually as frequency increases, which is related to the defect model [35, 37, 41]. Moreover, it is highly possible that the intrinsic frequency of the ceramics cannot keep pace with the change of electric field owing to the relaxation phenomenon. It is observed from Fig. 5b that Model A and Model B increased initially, and then decreased with various x. The dielectric loss of Model A and B are the maximum at $x = 40$ wt.% and $x = 30$ wt.%, respectively. It's possible because that the intrinsic frequency of ceramics keeps pace with the electric field frequency, resulting in the large loss. Electrical properties (dielectric properties and

Table 1 Exhibits ferroelectric, dielectric properties with various $SrTiO_3$ contents

Doped x contents (wt.%)	0	5	10	20	30	40	50
ε_r	9816	3770	2887	3060	2570	1450	879
$tan\delta$ (%)	0.81	0.34	0.46	0.88	1.12	0.97	0.97
P_r/ ($\propto$C/cm^2)	4.02	3.14	3.28	17.77	8.58	3.17	4.36
E_c/ (kV/mm)	0.36	0.37	0.41	2.52	1.60	1.93	2.15

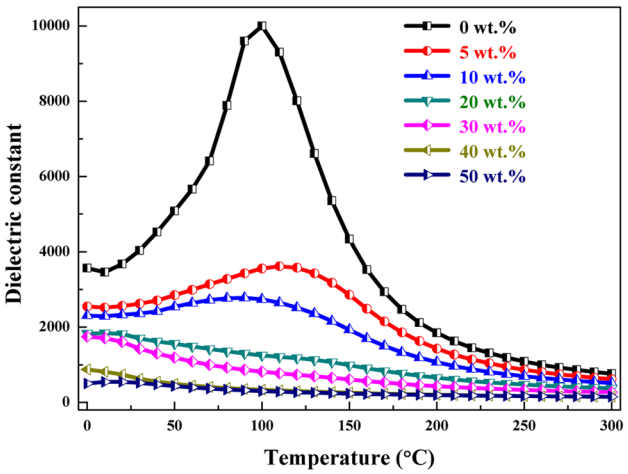

Fig. 6 Temperature dependence of dielectric constant and loss of $(Ba_{0.85}Ca_{0.15})(Zr_{0.08}Ti_{0.9}Sn_{0.02})O_3$-$x$SrTiO$_3$ ceramics at a frequency of 100 kHz

ferroelectric properties) of the ceramics with various $SrTiO_3$ contents are presented in Table 1.

3.3 Relaxor behavior and dielectric properties

Figure 6 shows the temperature dependence of dielectric constant for BCZTS-xST ceramics at the temperature range of 0–300 °C. In order to eliminate the influence of space-charge polarization at low frequency, the frequency of 100 kHz is selected. It is observed from Fig. 6 that ferroelectric–paraelectric phase transition temperature increased firstly, and then decreased. However, the phase transition temperature (T_m) of samples are not observed at the measured temperature range of 0–300 °C when 20 wt.% $\leq x \leq$ 40 wt.%. It is also observed from Fig. 6 that the phase transition temperature range around T_m became increasingly broad with the increase of x, which is called the diffuse phase transition. The diffuse phase transition is a typical characteristic of relaxor ferroelectrics. Another typical characteristic for

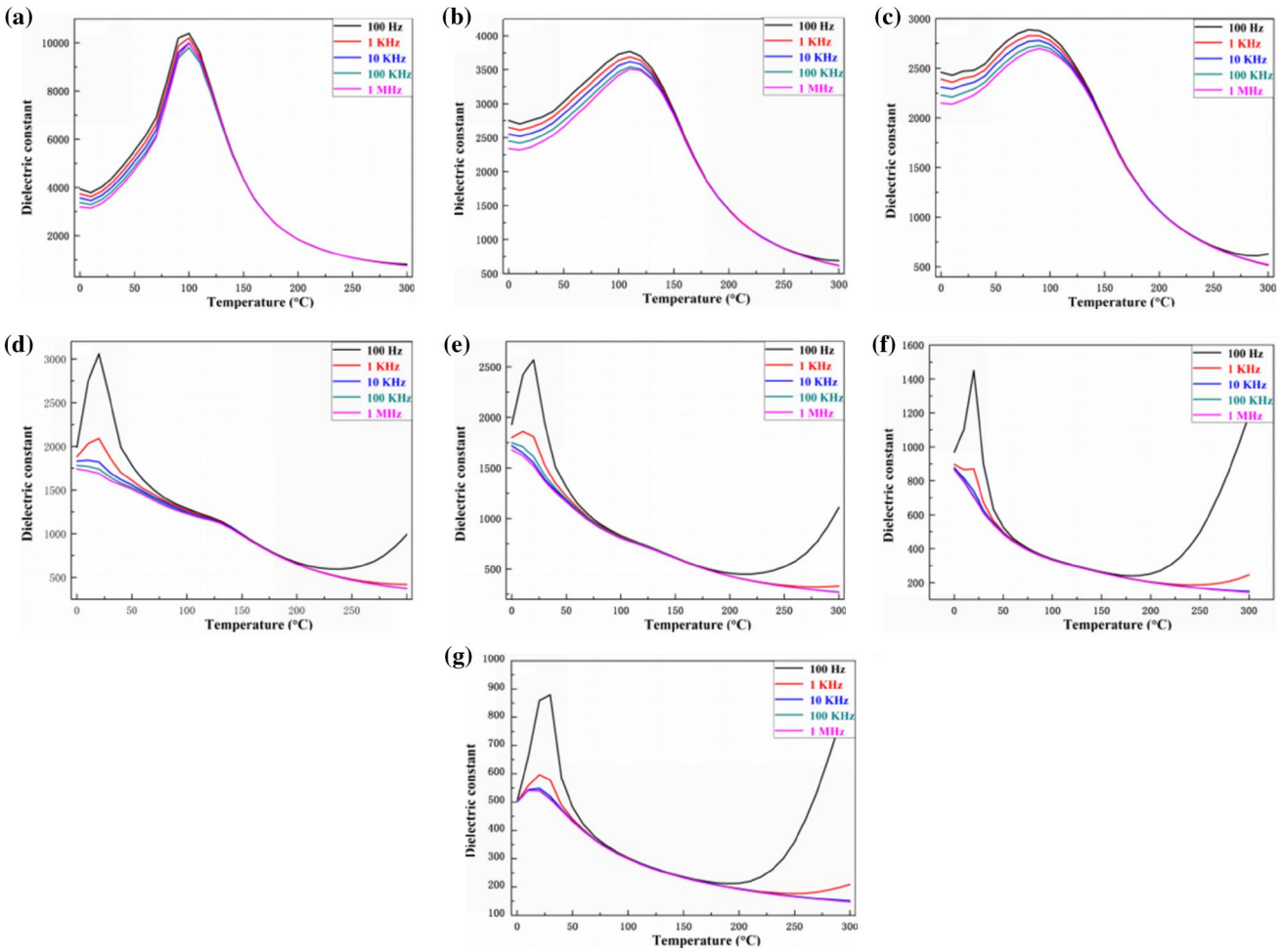

Fig. 7 Temperature dependence of dielectric constant of $(Ba_{0.85}Ca_{0.15})(Zr_{0.08}Ti_{0.9}Sn_{0.02})O_3$-$x$SrTiO$_3$ ceramics at various frequencies. **a** x = 0 wt.%, **b** x = 5 wt.%, **c** x = 10 wt.%, **d** x = 20 wt.%, **e** x = 30 wt.%, **f** x = 40 wt.%, **g** x = 50 wt.%

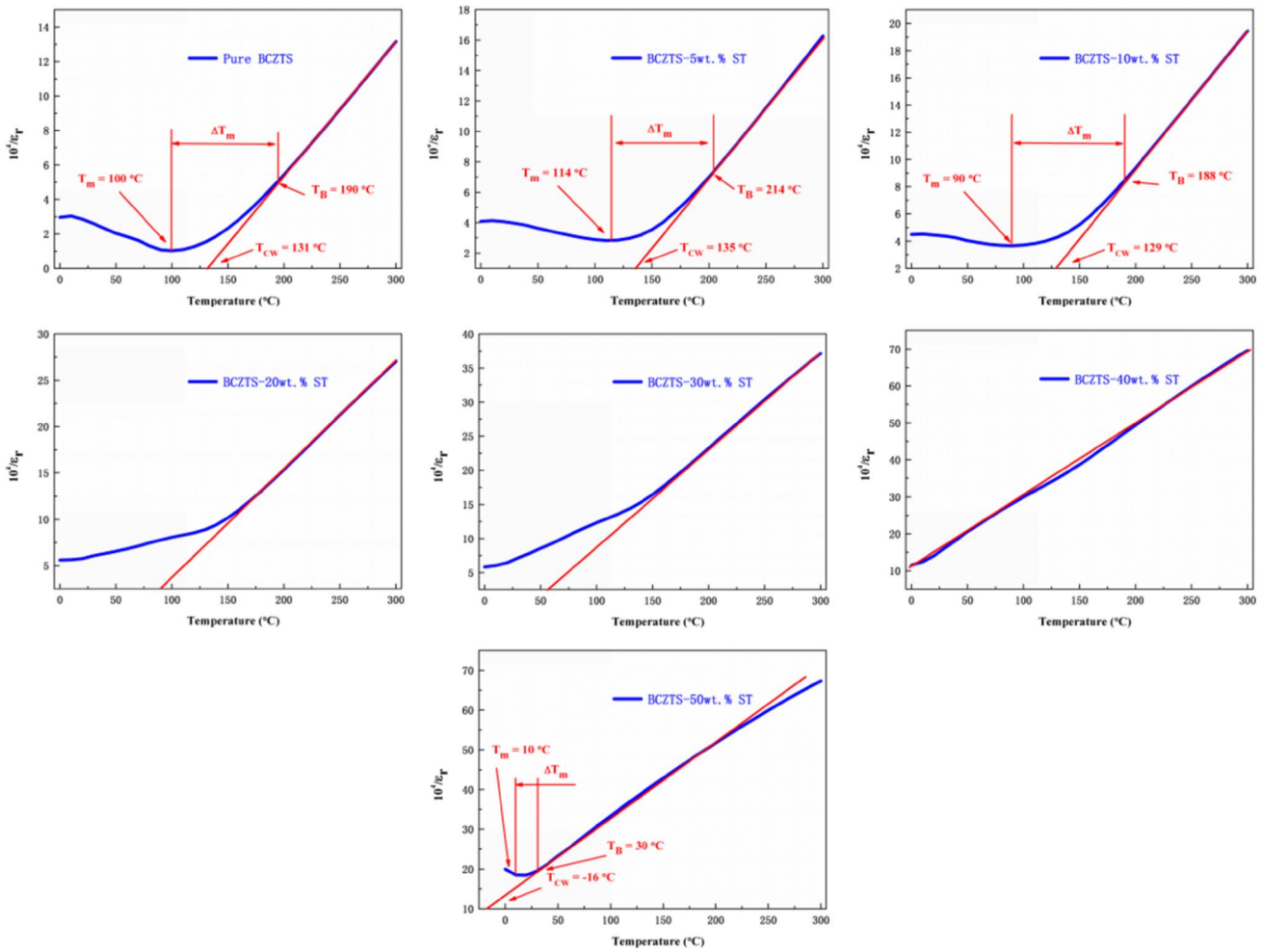

Fig. 8 The plot of inverse dielectric constant versus temperature for $(Ba_{0.85}Ca_{0.15})(Zr_{0.08}Ti_{0.9}Sn_{0.02})O_3$-$x$$SrTiO_3$ ceramics at a frequency of 100 kHz

the relaxor ferroelectrics is the frequency dispersion of the dielectric constant.

Figure 7 exhibits the temperature dependence of dielectric constant for BCZTS-xST ceramics at the various frequencies. As we can see, the ferroelectric-paraelectric transition happened at ~ 114 °C when $x = 5$ wt.%, and T_c increased compared with previous work [19]. For the relaxor ferroelectrics, it is widely believed that the frequency dispersion and the diffuse phase transition of dielectric permittivity are two typical characteristics. It is clearly observed from Fig. 7 that there is a strong frequency dispersion of dielectric constant. Hence, it can be concluded that the BCZTS-xST ceramics are indeed relaxor ferroelectrics. Furthermore, it is also observed from Fig. 7 that the dielectric constant increased at low frequency and high temperature with increasing of $SrTiO_3$ contents, which is mainly caused by space-charge and electrical conductivity [29]. The dielectric constants of BCZTS-xST ceramics at low temperature region (T_m) decreased with the increase of frequency, which also indicates that the BCZTS-xST ceramics is a typical relaxor ferroelectrics [29].

It is widely known that dielectric constant of the normal ferroelectrics should obey the Curie–Weiss law when the temperature exceeds the T_m, and it is described as follows:

$$\frac{1}{\varepsilon_r} = \frac{T - T_{CW}}{C} \quad (T > T_c) \tag{4}$$

where T_{cw} is the Curie–Weiss temperature and C is the Curie–Weiss constant which reflects the essence of ferroelectrics phase transition. To obtain the value of T_{cw}, the plot of the inverse dielectric constant versus temperature at 100 kHz is exhibited in Fig. 8. It is also seen from Fig. 8 that the phase transition temperature is not found at the measured temperature range when $x = 20$ wt.%, 30 wt.% and 40 wt.%, which is well corresponding to the analysis of Fig. 6. It is clearly observed that the dielectric constant obviously

Table 2 exhibits the T_{CW}, T_B, ΔT_m and γ for $(Ba_{0.85}Ca_{0.15})(Zr_{0.08}Ti_{0.9}Sn_{0.02})O_3$-$x$SrTiO$_3$ ceramics at 100 kHz

	$x=0$	$x=5$	$x=10$	$x=50$
T_B (℃)	190	214	188	30
γ	1.72	1.91	1.87	1.30
T_{cw} (℃)	131	135	129	16
$\Delta T_m = T_B - T_m$ (℃)	90	100	98	20
T_m (℃)	100	114	90	10

deviates from the Curie–Weiss law, and the deviation-degree can be defined as ΔT_m.

$$\Delta T_m = T_B - T_m \tag{5}$$

Where T_B denotes the temperature from which the dielectric constant starts to follow Curie–Weiss law, and T_m represents the temperature where dielectric constant reaches the maximum value. T_B can be obtained by fitting the function of the inverse dielectric constant versus temperature. It is seen from Table 2 that the ΔT_m is 100 °C at $x=5$ wt.%, which indicates that the diffuse phase transition behavior is the maximum here.

For the relaxor ferroelectrics, the function of the inverse dielectric constant versus temperature should obey the modified Curie–Weiss law, namely, the Uchino and Nomura function [42].

$$\frac{1}{\varepsilon_r} - \frac{1}{\varepsilon_m} = \frac{(T - T_m)^\gamma}{C} \tag{6}$$

where C is Curie constant, and ε_r represents the maximum value of dielectric constant; γ is called a diffuse constant ranging from 1 to 2. The ceramics are normal ferroelectrics at $\gamma=1$, and the ceramics are an ideal relaxor ferroelectrics at $\gamma=2$. However, the ceramics are relaxor ferroelectrics when $1<\gamma<2$. In order to further prove the effect of $SrTiO_3$ contents on the diffuse phase transition behavior of the BCZTS-xST ceramics, the plots of $\ln(T - T_m)$ as a function of $\ln(1/\varepsilon_r - 1/\varepsilon_m)$ at 100 kHz are shown in Fig. 9. Because the phase transition temperature was not found at the measured temperature range when $x=20$ wt.%, 30 wt.% and 40 wt.%. Therefore, their figures were not shown. It is observed from Fig. 9 that the diffuse behavior reaches the maximum value

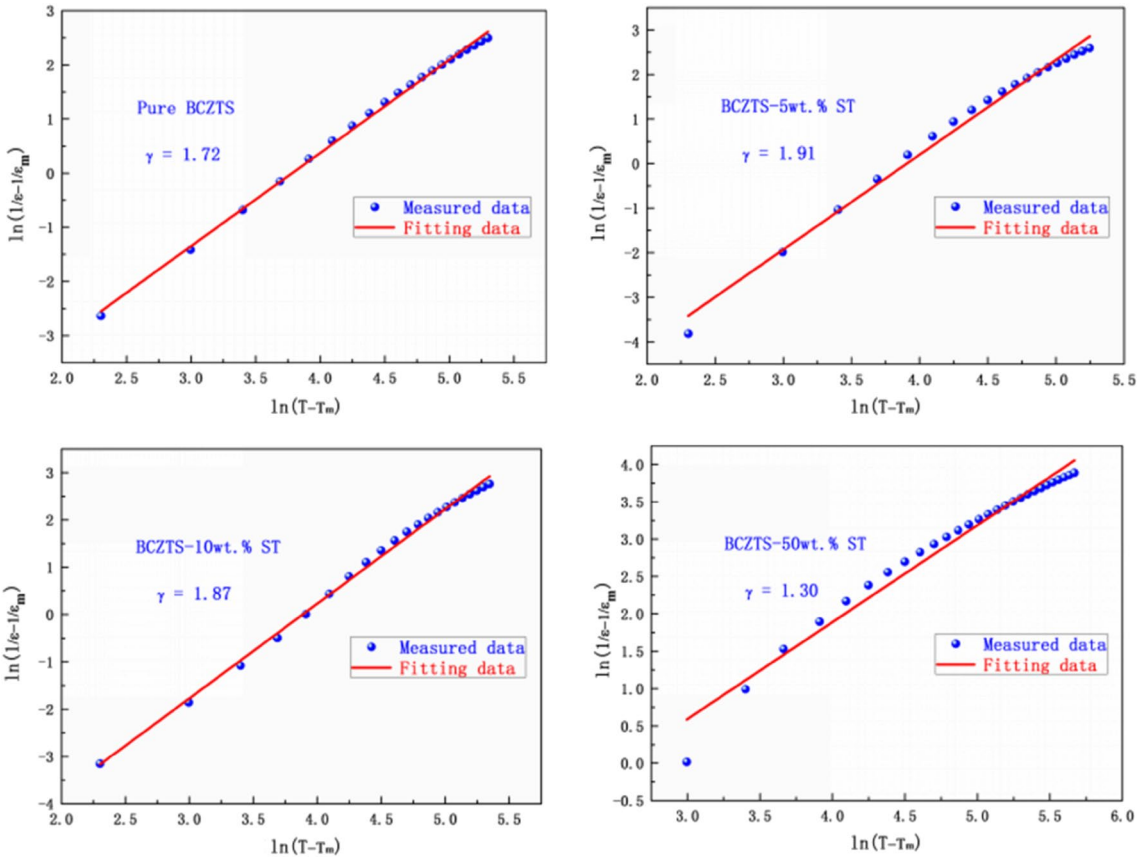

Fig. 9 The logarithm plot of reciprocal of dielectric constant and temperature for $(Ba_{0.85}Ca_{0.15})(Zr_{0.08}Ti_{0.9}Sn_{0.02})O_3$-$x$SrTiO$_3$ ceramics, the blue scatter and red solid line are measured data and fitting data, respectively. **a** $x=0$ wt.%, **b** $x=5$ wt.%, **c** $x=10$ wt.%, **d** $x=20$ wt.%, **e** $x=30$ wt.%, **f** $x=40$ wt.%, **i** $x=50$ wt.%

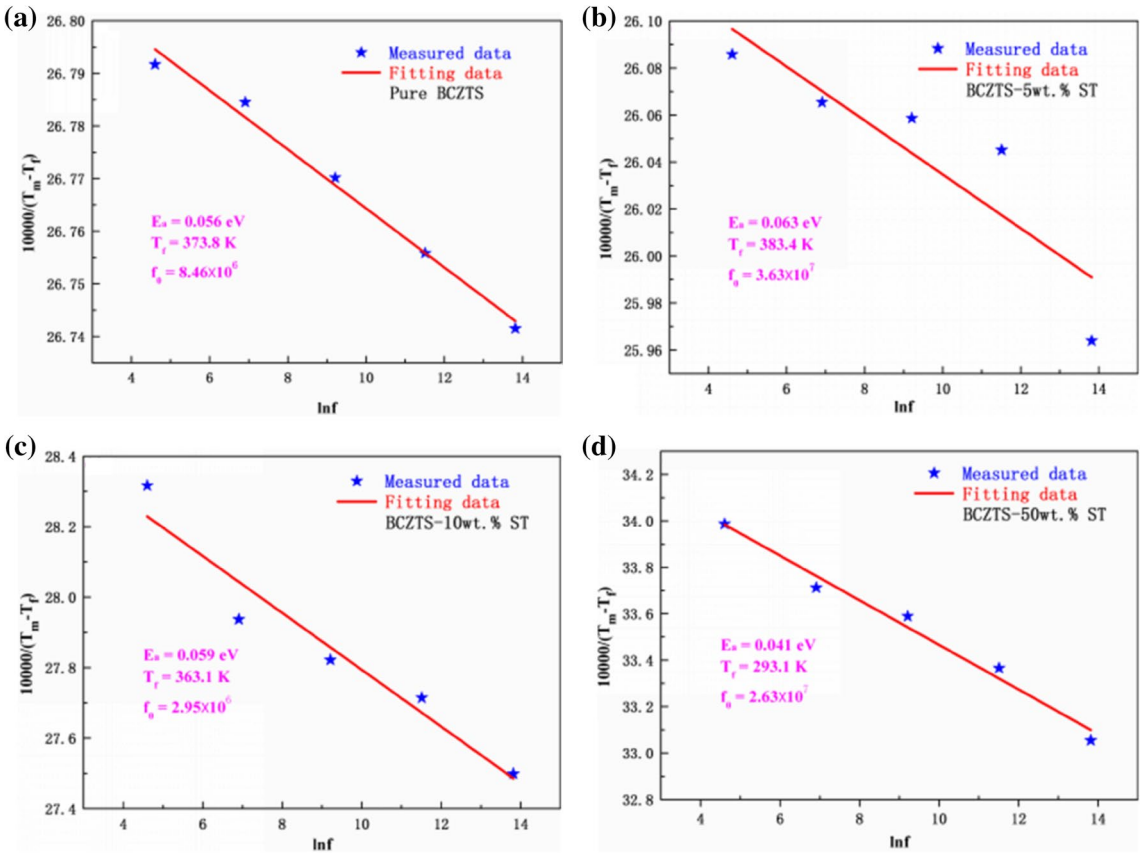

Fig. 10 Inverse of the difference between temperature of the dielectric maximum value (T_m) and the freezing temperature (T_f) as a function of ln$f$ for $(Ba_{0.85}Ca_{0.15})(Zr_{0.08}Ti_{0.9}Sn_{0.02})O_3$-$x$SrTiO$_3$ ceramics. (star: measured data, solid line: fitting to the Vogel–Fulcher law)

($\gamma = 1.91$) at $x = 5$ wt.%. ST is expected to be beneficial for the improvement of T_c and relaxor behavior of the ceramics, and the results suggest that relaxor behavior and T_c are indeed enhanced. T_c increase up about 21 °C. The probable reasons are discussed in detail in the work. The fitting data obtained by modified Curie–Weiss law are listed Table 2. It can be clearly seen that change of γ had the same change tendency to ΔT_m. Namely, γ and ΔT_m increased firstly, and then decreased.

Relaxation behavior can be explained by many theories such as super paraelectricity theory, random field model, the merging of micropolar regions into macropolar regions, and composition fluctuation theory [42, 43]. These models are based on the distortion of crystal structure which results in polar nanoregions (PNRs). Sn^{4+}(0.69 Å) and Sr^{2+}(1.12 Å) replaced Ti^{4+}(0.60 Å), Ca^{2+}(1.06 Å), Zr^{2+}(0.72 Å) and Ba^{2+} (1.38 Å). Due to their ion radius and ion valence are different, so local electric field and local elastic field were induced. These fields hindered the long-range dipole alignment, which gave rise to formation of PNRs and relaxation behavior [29, 43]. The relaxation behavior may be also caused by the interaction of PNRs and matrix.

It is well known that frequency dependence of the phase transition temperature (T_m) in the relaxor ferroelectrics can be described by a Vogel–Fulcher law, as shown in Eq. (7).

$$\ln f = \ln f_0 - E_a/k_B(T_m - T_f) \quad (7)$$

where E_a denotes activation energy and k_B is the Boltzmann constant. f_0 represents pre-exponential factor. T_f is the freezing temperature, i.e., where the dynamic behavior is no longer sufficient to reorient the polar nanodomains. Figure 10 shows the inverse ($T_m - T_f$) as a function of ln$f$ for BCZTS-xST ceramics. It is clearly observed that the measured data can be well fitted by the Vogel–Fulcher

Table 3 Shows the freezing temperature T_f, activation energy E_a and pre-exponential factor f_0 for $(Ba_{0.85}Ca_{0.15})(Zr_{0.08}Ti_{0.9}Sn_{0.02})O_3$-$x$SrTiO$_3$ ceramics

	$x=0$	$x=5$	$x=10$	$x=50$
E_a (eV)	0.056	0.063	0.059	0.041
f_0 (Hz)	8.46×10^6	3.63×10^7	2.95×10^6	2.63×10^7
T_f (℃)	373.8	383.4	363.1	293.1

law. For the BCZTS-xST ceramics, the values of E_a, f_0 and T_f can be obtained by fitting the measured data using the Vogel–Fulcher law. These values are listed at Table 3. It is observed that the activation energy reaches the maximum value ($E_a = 0.063$ eV) at $x = 5$ wt.%.

It is widely known that the activation energy is proportional to the volume of PNRs, so E_a can be regarded as one of dynamic driving powers for the formation of PNRs. It is observed that the ΔT_m changed with the change of E_a. The ΔT_m plays an important role to thermal driving power, which also provided an essential condition to the formation of PNRs. The interaction of activation energy and ΔT_m gave rise to the formation of PNRs, which resulted in the relaxation behavior. In conclusion, the relaxor behavior was originated from the combined action of the electric field, elastic field, activation energy and ΔT_m.

4 Conclusion

In summary, the $(Ba_{0.85}Ca_{0.15})(Zr_{0.08}Ti_{0.9}Sn_{0.02})O_3$-$x$$SrTiO_3$ ceramics were successfully prepared by conventional solid-state reaction method. The optimized ferroelectric properties are obtained at $x = 20$ wt.%, and the remnant polarization (P_r) and coercive field (E_c) are 11.67 μC/cm^2 and 2.06 kV/mm, respectively. The dielectric loss model and relaxor behavior are carefully discussed. The degree of relaxor, the Curie temperature and deviation-degree reach the maximum ($\gamma = 1.91$, $T_m = 114$ °C, $\Delta T_m = 100$, respectively) when $x = 5$ wt.%, and the results suggest that appropriate $SrTiO_3$ doping can enhance relaxor behavior of the ceramics. All these results indicate the $(Ba_{0.85}Ca_{0.15})(Zr_{0.08}Ti_{0.9}Sn_{0.02})O_3$-$x$$SrTiO_3$ ceramics are promising materials for multiferroic composite lead-free relaxor ferroelectrics with enhanced ferroelectric properties and relatively high T_c.

Acknowledgements The work is supported by High-level innovative talents plan of Guizhou province (no. (2015)4009) and specialized funds from industry and information technology department of Guizhou province (no. 201056). This work was also supported by the National Natural Science Foundation of China under Project no. 51602066.

References

1. H. Gene, Haertling, J. Am. Ceram. Soc. **82**, 797 (1999)
2. C.A. Randall, A. Kelnberger, G.Y. Yang, R.E. Eitel, T.R. Shrout, J. Electroceram. **14**, 177 (2005)
3. J. Rödel, W. Jo, K.T.P. Seifert, E.-M. Anton, T. Granzow, D. Damjanovic, J. Am. Ceram. Soc. **92**, 1153 (2009)
4. S.-T. Zhang, A.B. Kounga, E. Aulbach, H. Ehrenberg, J. Rödel, Appl. Phys. Lett. **91**, 112906 (2007)
5. J. Rödel, K.G. Webber, R. Dittmer, W. Jo, M. Kimura, D. Damjanovic, J. Eur. Ceram. Soc. **35**, 1659 (2015)
6. W. Li, Z. Xu, R. Chu, P. Fu, G. Zang, J. Alloys Compd. **583**, 305 (2014)
7. N. Ma, B.-P. Zhang, W.-G. Yang, D. Guo, J. Eur. Ceram. Soc. **32**, 1059 (2012)
8. J. Wu, Z. Fan, D. Xiao, J. Zhu, J. Wang, Prog. Mater Sci. **84**, 335 (2016)
9. Y.Y. Wang, L. Hu, Q.L. Zhang, H. Yang, Dalton Trans. **44**, 13688 (2015)
10. Y. Guo, Y. Liu, R.L. Withers, F. Brink, H. Chen, Chem. Mater. **23**, 219 (2011)
11. J. Wu, D. Xiao, J. Zhu, Chem. Rev. **115**, 2559 (2015)
12. T. Zheng, J. Wu, D. Xiao, J. Zhu, Prog. Mater Sci. **98**, 552 (2018)
13. W. Li, Z. Xu, R. Chu, P. Fu, P. An, Ceram. Int. **38**, 4353 (2012)
14. Z. Shen, X. Wang, H. Gong, L. Wu, L. Li, Ceram. Int. **40**, 13833 (2014)
15. H. Sun, Y. Zhang, X. Liu, Y. Liu, W. Chen, Ceram. Int. **41**, 555 (2015)
16. K. Xie, M. Toksoy, K. Kuwelkar, B. Zhang, J. krogstad, R. Haber, K. Hemker, J. Am. Ceram. Soc. **97**, 3710 (2014)
17. W. Bai, D. Chen, Y. Huang, B. Shen, J. Zhai, Z. Ji, J. Alloys Compd. **667**, 6 (2016)
18. J. Ma, X. Liu, W. Li, J. Alloys Compd. **581**, 642 (2013)
19. C. Han, J. Wu, C. Pu, S. Qiao, B. Wu, J. Zhu, D. Xiao, Ceram. Int. **38**, 6359 (2012)
20. X. Huang, R. Xing, C. Gao, Z. Chen, J. Rare Earths **32**, 733 (2014)
21. A. Hussain, A. Maqbool, J.S. Kim, T.K. Song, M.H. Kim, W.J. Kim, S.S. Kim, Int. J. Appl. Ceram. Technol. **12**, 228 (2015)
22. W. Liu, X. Ren, Rev. Lett. **103**, 257602 (2009)
23. N. Raengthon, T. Sebastian, D. Cumming, I.M. Reaney, D.P. Cann, J. Roedel, J. Am. Ceram. Soc. **95**, 3554 (2012)
24. W. Li, X. Liu, J. Ma, Y. Wu, Y. Cui, J. Mater. Sci. Mater. Electron. **24**, 1551 (2012)
25. S.B. Li, L.M. Zhang, C.B. Wang, X. Ji, Q. Shen, Ceram. Int. **42**, 18585 (2016)
26. G. Risse, B. Schlobach, W. Häßler, D. Stephan, T. Fahr, K. Fischer, J. Eur. Ceram. Soc. **19**, 125 (1999)
27. P. Chang, L. He, D. Wei, H. Wang, J. Eur. Ceram. Soc. **36**, 2519 (2016)
28. S. Schmidt, L. Ji, S. Keane, L. Bregante, D. Klenov, S. Stemmer, J. Am. Ceram. Soc. **88**, 789 (2005)
29. H.L. Du, W.C. Zhou, F. Luo, D.Z. Zhu, S.B. Qu, Z.B. Pei, J. Appl. Phys. **105**, 124104 (2009)
30. F.W. Van Keuls, R.R. Romanofsky, D.Y. Bohman, M.D. Winters, F.A. Miranda, C.H. Mueller, R.E. Treece, T.V. Rivkin, D. Galt, Appl. Phys. Lett. **71**, 3075 (1997)
31. X.L. Chao, J.J. Wang, P.F. Liang, T. Zhang, L.L. Wei. Z.P. Yang, Mater. Des. **89**, 465 (2016)
32. F.F. Zeng, Q.B. Liu, E.P. Cai, Y.Y. Wang, A. Xue, S.Q. Peng, S.L. Zhou, Y. Zhu, Ceram. Int. **44**, 10677 (2018)
33. P. Bhupaijita, C. Kornphoma, N. Vittayakorn, T. Bongkarn, Ceram. Int. **41**, s81 (2015)
34. H. Pan, Y. Hou, X. Chao, L. Wei, Z. Yang, Curr. Appl. Phys. **11**, 888 (2011)
35. Z. Yu, C. Ang, R. Guo, A.S. Bhalla, L.E. Cross, Appl. Phys. Lett. **80**, 1034 (2002)
36. C. Kornphom, N. Vittayakorn, T. Bongkarn, J. Mater. Sci. **51**, 4142 (2016)
37. C. Ang, A.S. Bhalla, R. Guo, L.E. Cross, Appl. Phys. Lett. **76**, 1929 (2000)
38. R. Viana, P. Lunkenheimer, J. Hemberger, R. Böhmer, A. Loidl, Phys. Rev. B **50**, 601 (1994)
39. W. Jo, S. Schaab, E. Sapper, L.A. Schmitt, H.-J. Kleebe, A.J. Bell, J. Rödel, J. Appl. Phys. **110**, 074106 (2011)

40. D. Robert, J. Wook, D. John, S. Silke, R. Jürgen, J. Am. Ceram. Soc. **94**, 4283 (2011)
41. C. Ang, L.E. Cross, Z. Yu, R. Guo, A.S. Bhalla, J.H. Hao, Appl. Phys. Lett. **78**, 2754 (2001)
42. Z.G. Ye, Key Eng. Mater. **81**, 155 (1998)
43. I.W. Chen, J. Phys. Chem. Solids **61**, 197 (2000)